

# Quantized Deep Path-following Control on a Microcontroller

Pablo Zometa<sup>1</sup> and Timm Faulwasser<sup>2</sup>

**Abstract**—Model predictive Path-Following Control (MPFC) is a viable option for motion systems in many application domains. However, despite considerable progress on tailored numerical methods for predictive control, the real-time implementation of predictive control and MPFC on small-scale autonomous platforms with low-cost embedded hardware remains challenging. While usual stabilizing MPC formulations lead to static feedback laws, the MPFC feedback turns out to be dynamic as the path parameter acts as an internal controller variable. In this paper, we leverage deep learning to implement predictive path-following control on microcontrollers. We show that deep neural networks can approximate the dynamic MPFC feedback law accurately. Moreover, we illustrate and tackle the challenges that arise if the target platform employs limited precision arithmetic. Specifically, we draw upon a post-stabilization with an additional feedback law to attenuate undesired quantization effects. Simulation examples underpin the efficacy of the proposed approach.

## I. INTRODUCTION

Nonlinear Model Predictive Control (NMPC) is a control method that can handle nonlinear system dynamics as well as input and state constraints. In its base variant NMPC for setpoint stabilization yields a static feedback law. Another variant is Model predictive Path-Following Control (MPFC), which has been successfully applied to motion control of robots to precisely follow a geometric reference path [1], [2], [3]. In MPFC the considered reference is a geometric path and timing along the path is computed at the run-time of the controller. Hence and in contrast to NMPC for setpoint stabilization, the MPFC is a dynamic feedback strategy as the reference position is an internal controller memory [4].

An often cited disadvantage of NMPC is its high computational cost, which significantly limits its use in low-cost computing hardware like MicroController Units (MCU). The Optimization Engine (OpEn) [5] and acados [6], two popular state-of-the-art NMPC solvers, can efficiently run on embedded hardware like a Raspberry Pi (a single-board computer). However, at the time of this writing, none of them can run out of the box on 32-bit MCUs.

To overcome the high computational demands of NMPC, the use of deep neural networks as a way to quickly find an approximate solution to the NMPC problem has been proposed [7], [8], [9]. In particular, [8] explores a robust multi-stage NMPC on an MCU using a Deep Neural Network (DNN) using single-precision floating-point arithmetic during network inference.

<sup>1</sup>PZ is with the Faculty of Engineering, German International University in Berlin, Germany. pablo.zometa@giu-berlin.de

<sup>2</sup>TF is with the Institute of Energy Systems, Energy Efficiency and Energy Economics, TU Dortmund, Germany. timm.faulwasser@ieee.org

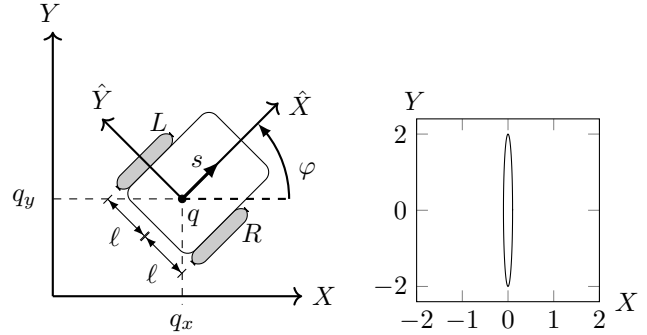


Fig. 1: Left: differential drive robot and its coordinate systems. Right: the path at scale, an ellipse. The robot's left and right wheels are marked  $L$  and  $R$ , respectively.

Moreover, to further increase the efficiency of DNNs, the use of quantization—i.e., storing the network parameters using fixed-point representation instead of floating point—has been explored [10]. Compared to a regular DNN, a quantized DNN executes much faster, requires less memory, and is more energy efficient—there is the downside of some loss of numerical accuracy [10].

The present paper investigates the use of quantized deep neural networks for model predictive path-following control of mobile robots. Our main contribution is two-fold: first, we propose a way to generate the training set that takes into account the path to be followed, and second, we extend the DNN with a simple controller to make up for errors introduced by the quantized DNN approximation.

Using the proposed approach with hardware-in-the-loop simulations running on an MCU, we show that a quantized deep neural network requiring less than 5 kB of storage memory achieves a good path following performance while being several orders of magnitude faster than OpEn.

The remainder of the paper is organized as follows: Section II recalls MPFC applied to a mobile robot. Section III discusses quantized DNNs. Section IV introduces an approach to efficiently approximate the MPFC problem using quantized DNN, followed by the results (Section V) and conclusions (Section VI).

## II. PATH FOLLOWING CONTROL OF A MOBILE ROBOT

This section summarizes the main idea of MPFC according to [11], and its application to differential drive robots [3].

### A. System Description

Fig. 1 shows a schematic of a differential drive robot. The global (inertial) frame is defined by the axes  $XY$ ,

whereas the local frame attached to the robot is defined by the axes  $\hat{X}\hat{Y}$ . The position of the robot in the global frame is represented by the Cartesian coordinates of point  $q$  (the origin of the local frame). The robot's pose  $\xi$  in the inertial frame is represented by its Cartesian position  $q = [q_x \ q_y]^T$  and orientation  $\varphi$ , that is  $\xi = [q_x \ q_y \ \varphi]^T$ . We represent the robot dynamics as the rate of change of the pose in terms of the robot's forward speed  $s$ , and its angular velocity  $\omega$ :

$$\dot{\xi} = f(\xi, u) = \begin{bmatrix} s \cos(\varphi) \\ s \sin(\varphi) \\ \omega \end{bmatrix}, \quad \xi(0) = \xi_0, \quad (1)$$

with  $\xi \in \mathcal{X} \subseteq \mathbb{R}^3$ , and  $u = [s \ \omega]^T \in \mathcal{PC}(\mathcal{U}) \subset \mathbb{R}^2$ . We use  $\mathcal{PC}(\mathcal{U})$  to denote that the inputs are piece-wise continuous and take values from a compact set  $\mathcal{U}$ .

### B. The State-Space Path-Following Problem

We recall the path-following problem in the state space of the robot model (1) as introduced by [11]. The path-following problem aims at making the system (1) follow a geometric reference without explicit timing requirements, i.e., *when to be where* on the path is not specified. The reference is given by

$$\mathcal{P} = \{\xi \in \mathbb{R}^3 \mid \exists \theta \in \mathbb{R} \mapsto \xi = p(\theta)\}.$$

The variable  $\theta(t) \in \mathbb{R}$  is the path parameter, and  $p(\theta(t)) \in \mathbb{R}^3$  is a parameterization of  $\mathcal{P}$ . Note that although  $\theta$  is dependent on time, its time evolution  $t \mapsto \theta$  is not specified. Thus, the control inputs  $u \in \mathcal{PC}(\mathcal{U})$  and the timing  $\theta: \mathbb{R}_0^+ \rightarrow \mathbb{R}_0^+$  are chosen such that they follow the path as closely as possible.

*Problem 1. (State-space path following with speed assignment)*

- 1) Convergence to the path: the robot's state  $\xi$  converges to the path  $\mathcal{P}$  such that

$$\lim_{t \rightarrow \infty} \|\xi(t) - p(\theta)\| = 0.$$

- 2) Constraint satisfaction: the constraints on the states  $\xi \in \mathcal{X}$  and inputs  $u \in \mathcal{U}$  are satisfied at all times.
- 3) Velocity convergence: the path velocity  $\dot{\theta}$  converges to a predefined profile such that

$$\lim_{t \rightarrow \infty} \|\dot{\theta}(t) - v_r(t)\| = 0.$$

Here we consider path parametrizations of the form

$$p(\theta) = [p_x(\theta) \ p_y(\theta) \ p_\varphi(\theta)]^T, \quad (2)$$

$$p_\varphi(\theta) = \arctan\left(\frac{p'_y}{p'_x}\right), \quad p'_x = \frac{\partial p_x}{\partial \theta}, \quad p'_y = \frac{\partial p_y}{\partial \theta},$$

where  $p_x(\theta)$  and  $p_y(\theta)$  are at least twice continuously differentiable (see [3]). We denote  $p_{xy} = [p_x \ p_y]^T$  as the vector of Cartesian coordinates of the path.

The path parameter  $\theta$  is considered a virtual state, which is controlled by the virtual input  $v$ . Here the dynamics of  $\theta$  are chosen as a single integrator:

$$\dot{\theta} = v, \quad \theta(0) = \theta_0,$$

where  $v \in \mathcal{PC}(\mathcal{V})$ ,  $\mathcal{V} \doteq [0, \bar{v}]$ , and  $\bar{v} \in \mathbb{R}$ .

The path following problem is formulated using the augmented system

$$\dot{z} = f(z, w) = \begin{bmatrix} \dot{q}_x \\ \dot{q}_y \\ \dot{\varphi} \\ \dot{\theta} \end{bmatrix} = \begin{bmatrix} s \cos(\varphi) \\ s \sin(\varphi) \\ \omega \\ v \end{bmatrix},$$

with the augmented state vector  $z = [\xi^T \ \theta]^T = [q_x \ q_y \ \varphi \ \theta]^T \in \mathcal{Z} = \mathcal{X} \times \mathbb{R}_0^+$  and the augmented input vector  $w = [u^T \ v]^T \in [s \ \omega \ v]^T \in \mathcal{PC}(\mathcal{U} \times \mathcal{V}) \subset \mathbb{R}^3$ .

System (1) is *differentially flat*, and  $[q_x \ q_y]^T$  is one of its flat outputs [12]. Therefore there is an input  $u_r = [s_r \ \omega_r]$  which guarantees that path (2) is followed by the system.

The vector  $u_r$  is used as a reference for the input vectors and can be built by observing that the first two equations of system (1) satisfy  $s^2 = \dot{q}_x^2 + \dot{q}_y^2$ , and thus:

$$s_r(\theta, v) = \sqrt{\left(\frac{dp_x(\theta(t))}{dt}\right)^2 + \left(\frac{dp_y(\theta(t))}{dt}\right)^2} = v \sqrt{(p'_x)^2 + (p'_y)^2}. \quad (3)$$

Furthermore, from the last equation of system (1) we have  $\omega = \dot{\varphi}$ , which yields

$$\begin{aligned} \omega_r(\theta, v) &= \frac{dp_\varphi(\theta(t))}{dt} \\ &= v \left( (p'_x)^2 + (p'_y)^2 \right)^{-1} (p'_x p''_y - p'_y p''_x), \quad (4) \\ &\text{with } p''_x = \frac{\partial^2 p_x}{\partial \theta^2}, \text{ and } p''_y = \frac{\partial^2 p_y}{\partial \theta^2}. \end{aligned}$$

Further details on the derivation can be found in [13], [3].

### C. Model Predictive Path Following Control (MPFC)

This section is based on the state-space MPFC scheme proposed in [11]. For paths defined in output spaces, we refer to [4], [2].

The sampling period is  $\delta > 0$ , and the prediction horizon is  $T = N\delta$ , with  $N \in \mathbb{N}$ . The extended state at the current sampling time  $t_k = k\delta$  is denoted  $z_k = [\xi(t_k) \ \theta(t_k)]$  and the extended control input is  $w = [u \ v]$ . We consider the stage cost

$$\ell(z, w) = \left\| \begin{bmatrix} \xi - p(\theta) \\ \theta \end{bmatrix} \right\|_Q^2 + \left\| \begin{bmatrix} u - u_r(\theta, v) \\ v - v_r \end{bmatrix} \right\|_R^2,$$

with  $Q = Q^T \succeq 0$  and  $R = R^T \succ 0$ , i.e., symmetric positive (semi)definite diagonal matrices. The Optimal Control Problem (OCP) to be solved repeatedly at each sampling instant  $t_k$  and using  $z_k$  as parametric data reads

$$\begin{aligned} \mathbf{w}^* &= \arg \min_{w \in \mathcal{PC}(\mathcal{W})} \int_0^T \ell(z(\tau), w(\tau)) d\tau \\ &\text{subject to } \dot{z}(\tau) = f(z(\tau), w(\tau)), \quad z(0) = z_k, \\ &\quad z(\tau) \in \mathcal{Z}, \quad w(\tau) \in \mathcal{W}. \end{aligned} \quad (5)$$

Although this OCP is formulated in continuous time, our MPFC *implementation* is done in discrete time with  $\mathbf{w}^* =$

$\{w_0^*, \dots, w_{N-1}^*\} \in \mathcal{W}^N$  a sequence of  $N$  input vectors. Typically, in MPC we only apply to the controlled system the first vector  $w = w_0^*$  in the sequence  $\mathbf{w}^*$ . The MPFC feedback controller based on (5) can be expressed as the function

$$w = \begin{bmatrix} u \\ v \end{bmatrix} = \mathbb{M}(z). \quad (6)$$

Observe that  $w$  entails the robot command  $u$  and the virtual control  $v$ , which controls the evolution of the path parameter  $\theta$ , cf. (II-B). Hence only  $u$  is applied to the robot.

### III. FEEDFORWARD NEURAL NETWORKS

Next, we recall the basics of how a function can be approximated by feedforward neural networks, the advantages of using deep architectures, and how to quantize them.

#### A. Deep Neural Networks

The use of feedforward Neural Networks (NN) is motivated by their universal function approximation properties [14]. In particular, we are interested in approximating the MPFC feedback (6). Our goal is to train an NN that approximates  $\mathbb{M}(z)$  by defining the mapping  $w^D = \mathbb{D}(z; \Theta)$ , where  $\Theta$  represents a set of  $N_\Theta$  unknown parameters, which are learned during *training*. Once we have a trained network, we can use the  $\mathbb{D}(z; \Theta)$  to *infer* the values of  $w^D \approx \mathbb{M}(z)$ .

To train our network, we rely on a training data set

$$\mathcal{T} = \{\nu^1, \nu^2, \dots, \nu^{N_T}\}, \text{ with } \nu^j = \begin{bmatrix} z^j \\ \mathbb{M}(z^j) \end{bmatrix} \in \mathbb{R}^7,$$

$j \in \mathcal{J} = \{1, \dots, N_T\}$ , and  $N_T$  is large enough. The training algorithm aims to find the values of  $\Theta$  that make  $\mathbb{D}(z^j; \Theta) \approx \mathbb{M}(z^j), \forall j \in \mathcal{J}$  using some statistical measure like the Mean Squared Error (MSE). It is common to use a gradient-based optimization algorithm during training to minimize the MSE. The trained network is said to *generalize* well if  $\mathbb{D}(z; \Theta)$  is still a good approximation of  $\mathbb{M}(z)$  for values of  $z$  not seen during training, in particular those relevant to the application.

In general, an NN consists of  $H+2$  layers: one input layer, one output layer, and  $H \geq 1$  hidden layers. Each layer  $k$  consists of  $n_k$  units called neurons. Commonly, if there are only one or two hidden layers, the network is referred to as *shallow*, otherwise, it is called a *Deep Neural Network* (DNN). The advantage of a DNN, compared to a shallow network, is that it can approximate a function like (6) with similar accuracy but with fewer parameters  $N_\Theta$  as fewer neurons (and hence parameters) are considered per layer. We refer to [15] for details.

Starting with the input  $z = h^0$  as the first layer, the output of layer  $k = 1, 2, \dots, H+1$  is

$$h^k = \beta(b^k + W^k h^{k-1}), \quad (7)$$

with  $b^k \in \mathbb{R}^{n_k}$  a vector called *bias* and  $W^k \in \mathbb{R}^{n_k \times n_{k-1}}$  a matrix called *weights*, and the function  $\beta(\cdot)$  is a saturating *activation* function. The last layer is the output layer  $w^D =$

$h^{H+1}$ . Note that  $\Theta = \{b^1, W^1, \dots, b^{H+1}, W^{H+1}\}$ , and the number of parameters of the network is given by:

$$N_\Theta = \sum_{k=1}^{H+1} n_k(1 + n_{k-1}).$$

For example, a network with 1 hidden layer would be described as  $w^D = \mathbb{D}(z; \Theta) = \beta(b^2 + W^2 \beta(b^1 + W^1 z))$ .

A frequently used activation function is the Rectifying Linear Unit (ReLU) ([15, p. 171]), defined as  $\beta(h) = \max(\mathbf{0}, h)$ , where  $\max(\cdot)$  is computed element-wise. Other common activation functions include the tangent hyperbolic and the sigmoid function.

#### B. Network Training

In practice, to find the set of parameters  $\Theta$  that make  $\mathbb{D}(\cdot)$  approximate  $\mathbb{M}(\cdot)$  sufficiently well the higher-level set of so-called *hyper-parameters* needs to be determined. Common hyper-parameters include the network architecture ( $H, n_k, \beta$ ), and the gradient-based optimization algorithm parameters (e.g., the step size, also called the *learning rate*) to name just a few. A suitable combination of hyper-parameters is typically determined experimentally [16].

It is helpful to normalize the training set to improve the numerical properties of the network. Here, we represent the training set as a matrix  $\mathcal{T} \in \mathbb{R}^{7 \times N_T}$  for simplicity in notation. For each column  $j$ , and row  $i$  of  $\mathcal{T}$  we have:

$$\bar{\nu}_i^j = N(\nu_i^j; \mu_i, \sigma_i) = \frac{\nu_i^j - \mu_i}{\sigma_i},$$

where  $\mu_i$  is the mean and  $\sigma_i$  is the standard deviation of row  $i$ . Note that  $\nu^j$  represents column  $j$  of  $\mathcal{T}$ . After applying this transformation, we obtain a normalized data set  $\bar{\mathcal{T}}_N$  that has each row  $i$  with  $\bar{\mu}_i = 0$  and  $\bar{\sigma}_i = 1$ . To recover the original set  $\mathcal{T}$ , we apply the inverse transformation:

$$\nu_i^j = N^{-1}(\bar{\nu}_i^j; \mu_i, \sigma_i) = \bar{\nu}_i^j \sigma_i + \mu_i.$$

These operations must be applied to the extended robot state  $z = [\xi \ \theta] \in \mathbb{R}^4$  and the extended input vector  $w^D = [u \ v] \in \mathbb{R}^3$  during inference. That is  $\bar{z}_i = N(z_i; \mu_i, \sigma_i)$ , for  $i = 1, 2, 3, 4$ , and  $w_i^D = N^{-1}(\bar{w}_i; \mu_{i+4}, \sigma_{i+4})$ , for  $i = 1, 2, 3$  (refer to Fig. 4a).

#### C. Quantized DNN (QDNN)

Quantization refers to storing the parameters of the network (weights and biases) as integer values. The main advantages are reduced memory required to store the  $N_\Theta$  parameters, faster execution, and higher energy efficiency during inference. The main disadvantage is the loss of accuracy in the inference [10].

It is common to use an 8-bit integer representation (i8) to store the parameters set  $\Theta$ . The network is trained first using floating point numbers often with single precision (32 bits). After the training is completed, the parameters  $\Theta$  are *quantized* to an i8 approximation. There are different quantization methods [10]. Here we have used a uniform asymmetric quantization. That means that during inference,

the *normalized* inputs  $\bar{z}$  in the network must be transformed from a floating point number to an integer using

$$\hat{z} = Q(z; \tilde{a}, \hat{b}) = \text{i8}(\tilde{a}\bar{z}) + \hat{b}, \quad (8)$$

where  $\tilde{a}$  is a floating point scaling,  $\hat{b}$  is an integer offset, and  $\text{i8}$  refers to a mapping from floating point to 8-bit integer representation. Similarly, the output of the network  $\hat{w}$  must be transformed from an 8-bit integer to a floating-point normalized output  $\bar{w}$ , i.e., it must be *dequantized* using

$$\bar{w} = Q^{-1}(\hat{w}; \tilde{c}, \hat{d}) = \text{f32}(\hat{w} - \hat{d})\tilde{c}, \quad (9)$$

where  $\tilde{c}$  is a floating point scaling,  $\hat{d}$  is an integer offset, and  $\text{f32}$  refers to a mapping from an 8-bit integer to a single-precision floating-point representation. The scaling and offset parameters are determined during the quantization of  $\Theta$ . Fig. 4a depicts how the robot state  $z$  (input to the network) and input vector  $w^D$  (output of the network) are numerically transformed.

#### IV. QDNN-BASED MPFC

We now turn to a practical approach to approximate the MPFC problem presented in Section II using QDNNs as described in Section III. We denote this approach as MPFC-QDNN. This section also discusses how to augment the MPFC-QDNN with an online feedback controller to improve the accuracy of the path-following control. We denote this approach as MPFC-QDNN+P.

##### A. Generating a Training Set for MPFC

Although it is possible to find a network that approximates  $\mathbb{M}(z) \forall z \in \mathcal{Z}$ , this typically would require a network and set  $\mathcal{T}$  larger than necessary for the path-following problem. Under normal circumstances, a mobile robot following a path will mostly take poses  $\xi$  that are close to the reference path  $p(\theta)$ . Based on this, a smaller set  $\mathcal{Z}_C \subset \mathcal{Z}$  can be used to significantly reduce the size of the network and the training set, without affecting the performance of the MPFC near the path. However, if the robot is driven far away from the path (e.g., due to large disturbances), the MPFC-QDNN may not be able to bring the robot back to following the path.

To generate a set  $\mathcal{T}$  appropriate for MPFC, we propose to use a corridor centered around the path (see Fig. 2). To build the set  $\mathcal{T}$ , we select specific values of the path parameter  $\theta_i$ ,  $i = 0, 1, \dots, N_p$ , and compute the path vector  $p(\theta_i)$ . At each  $\theta_i$ , we build a corridor  $C(\theta_i) \in \mathbb{R}^{3 \times N_c}$  using a set of  $N_c$  points in the vicinity of  $p(\theta_i)$ .

We propose a corridor in the form of a cuboid centered around  $p(\theta_i)$  along the orthonormal vectors  $\vec{t}, \vec{n}, \vec{o}$  (see Fig. 2), with width  $2c_W$ , length  $2c_L$ , and height  $2c_H$ . The points  $C^j(\theta) = [p_t^j \ p_n^j \ p_o^j]^\top$  are equidistant along each axis, with

$$\begin{bmatrix} -c_W \vec{t} \\ -c_L \vec{n} \\ -c_H \vec{o} \end{bmatrix} \leq \begin{bmatrix} p_t^j \\ p_n^j \\ p_o^j \end{bmatrix} \leq \begin{bmatrix} c_W \vec{t} \\ c_L \vec{n} \\ c_H \vec{o} \end{bmatrix}.$$

The set  $\mathcal{Z}_C$  has  $N_p N_c$  elements. The corridor can be defined in many different ways (e.g., using randomly selected points inside an ellipsoid). Here we have presented one way

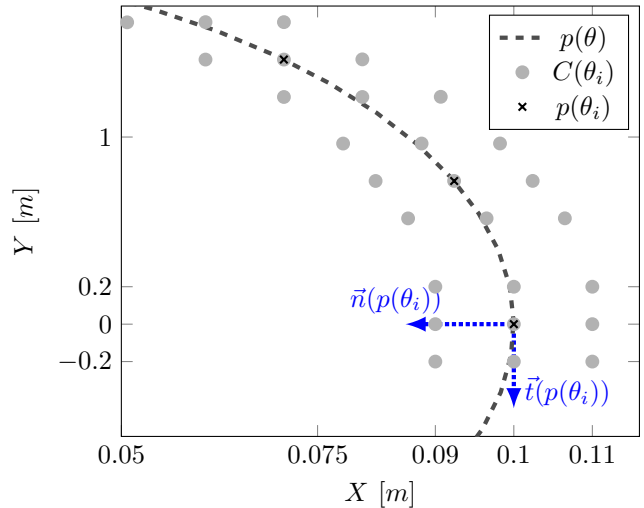


Fig. 2: Simplified 2-dimensional visualization of data point used to build the training set  $\mathcal{T}$ . The vectors  $\vec{n}, \vec{t}, \vec{o}$  (coming out of the page) are orthonormal. Only  $p_x$  and  $p_y$  are shown (the orientation  $p_\varphi$  is not depicted). The figure shows the corridor for three values of  $\theta_i$ , and at each point  $p(\theta_i)$  (cross) a corridor  $C(\theta_i)$  of 9 points (dots) is constructed. The width (0.02 m in the figure), and the length (0.4 m) of the corridor are measured normal (along  $\vec{n}$ ) and tangential (along  $\vec{t}$ ) to the path at  $p(\theta_i)$ , respectively.

that has worked well in our experiments (a cuboid grid with equidistant points). Determining the optimal way to construct the set  $\mathcal{Z}_C$  is beyond the scope of this work.

The size of the corridor plays an important role in how well the MPFC-QDNN can follow the path in practice. If the corridor is too narrow, the network is not able to follow the path at all, due to inevitable errors inherent in any feedback control system. A broad corridor is thus preferred. However, that may require more data points in the set, and perhaps a larger network, to make the approximation  $\mathbb{D}(\cdot)$  useful.

##### B. Path-Following Error

Although MPFC can follow the reference path  $\mathcal{P}$  very accurately, at any time  $t$  there might be an error  $e$  in the robot's Cartesian position  $q(t)$  with respect to the reference point in the path  $p(\theta(t))$ . In the  $XY$  coordinates, the error is given by:

$$e_{XY}(q(t), p_{xy}(\theta(t))) = q(t) - p_{xy}(\theta(t)).$$

This error vector can be expressed in the basis formed by the orthonormal vectors  $\vec{t}(p_\varphi(\theta))$  and  $\vec{n}(p_\varphi(\theta))$ , which are tangential and normal to the path at  $p_{xy}(\theta)$ , respectively (refer to Fig. 3). That is:

$$e(q(t), p(\theta(t))) = e_n(q, p)\vec{n}(p_\varphi) + e_t(q, p)\vec{t}(p_\varphi), \quad (10)$$

where the scalars  $e_n$  and  $e_t$  are the projection of  $e_{XY}$  onto each orthonormal vector, computed by the dot product

$$\begin{aligned} e_n(q, p) &= (q - p_{xy})^\top \vec{n}(p_\varphi), \\ e_t(q, p) &= (q - p_{xy})^\top \vec{t}(p_\varphi). \end{aligned}$$

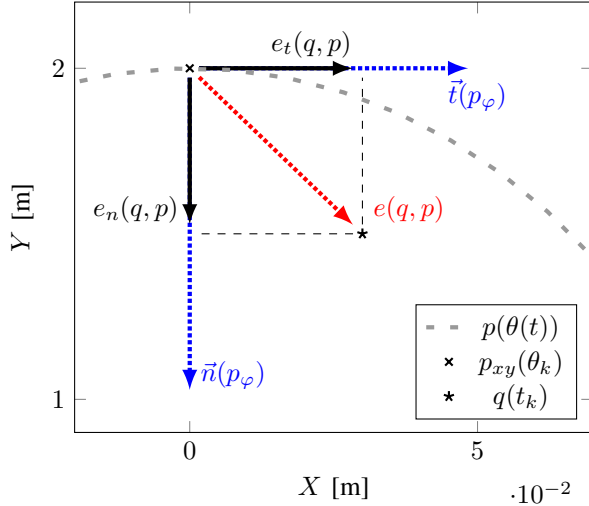


Fig. 3: At any given time  $t_k$ , the robot's position in the global frame  $XY$  is given by  $q(t_k)$ . The unit vectors  $\vec{t}(\theta_k)$  (not shown at scale), and  $\vec{n}(\theta_k)$  are tangential and normal to the path at point  $p_{xy}(\theta_k)$ , respectively, and  $\theta_k = \theta(t_k)$ . The vector  $e(q, p) = q - p_{xy} = e_t(q, p)\vec{t}(p_\varphi) + e_n(p, q)\vec{n}(p_\varphi)$  is the current robot's position with respect to the path.

In the case of an ellipse, the tangential and normal vectors are given by:

$$\vec{t}(p_\varphi) = \begin{bmatrix} \cos(p_\varphi) \\ \sin(p_\varphi) \end{bmatrix}, \quad \vec{n}(p_\varphi) = \begin{bmatrix} -\sin(p_\varphi) \\ \cos(p_\varphi) \end{bmatrix}.$$

### C. Augmented Control Scheme

Due to the MPFC-QDNN being an approximation of the MPFC, the path-following error  $e$  resulting from  $\mathbb{D}(z; \Theta)$  is significantly larger than the error observed under the original MPFC controller  $\mathbb{M}(z)$  (see Section V). To compensate this error we extend the MPFC-QDNN controller with an additional linear feedback which acts on the tangential component  $e_t$  through the forward speed of the robot  $s$ , and on the normal component  $e_n$  through the robot's angular speed  $\omega$ . Put differently, the compensation term  $w^P$  is added to the control vector, i.e.,  $w = w^D + w^P$ . Here  $w^P = [s^P \ \omega^P \ 0]^T$ , with  $s^P = P_t e_t$ , and  $\omega^P = P_n e_n$ , where  $P_t$ , and  $P_n$  are the proportional gains (see Fig. 4). We denote this approach MPFC-QDNN-P. We selected static feedback mainly due to its simplicity and effectiveness as shown in Section V.

### D. Implementation

We consider an ellipse as the path (see Fig. 1), which is defined by the parametrization

$$p(\theta) = \left[ 0.1 \cos(\theta) \quad 2 \sin(\theta) \quad \arctan\left(\frac{-0.1 \sin(\theta)}{2 \cos(\theta)}\right) \right]^T,$$

which yields the input references (3) and (4) as

$$s_r(\theta, v) = 2v \sqrt{1 - 0.9975 \sin^2(\theta)},$$

$$\omega_r(\theta, v) = 2v (40 - 39.9 \sin^2(\theta))^{-1}.$$

To generate the training set  $\mathcal{T}$ , we use a corridor consisting of a cuboid of width  $2c_W = 0.02$ , length  $2c_L = 0.2$ , and

height  $2c_H = \frac{2\pi}{3}$ . Each axis is split into 5, 5, and 40 equidistant points ( $N_c = 1000$ ), respectively. We split the path in  $N_p = 4000$  equidistant segments between  $0 \leq \theta \leq 2\pi$ , which corresponds to a full turn around the path. The subset of states in the corridor  $\mathcal{Z}_C$  consists of  $N_p N_c = 4E6$  points.

To solve the MPFC problem (5), and consequently find  $w = \mathbb{M}(z)$ ,  $\forall z \in \mathcal{Z}_C$  according to (6), we use the Optimization Engine (OpEn) [5], a fast solver for optimal control problems. The training set  $\mathcal{T}$  consists of  $N_p N_c$  pair of vectors  $z$ ,  $\mathbb{M}(z)$  for all  $z \in \mathcal{Z}_C$ . We use a discretization time  $\delta = 0.01$  s, and a horizon length  $T = 0.6$  s in (5).

We use a random search approach to find the hyper-parameters of a network that is a good approximation to  $\mathbb{M}$  under the constraint that the number of parameters  $N_\Theta$  should remain *small*. i.e., to reduce the size of the network in the MCU's ROM. Random search typically delivers better results than manual or grid search for the same amount of computation during training [16]. The selected hyper-parameters were the number of hidden layers  $H$ , the number of units in each hidden layer  $n_k$ ,  $k = 1, \dots, H$ , and the learning rate of the optimization algorithm (see the Appendix). To find the hyper-parameters we use KerasTuner [17]. To perform the training and the quantization of the network we use the deep learning framework Keras/TensorFlow [18], [19].

We implement a Hardware-In-the-Loop (HIL) simulation where the MPFC-QDNN+P is deployed on an STM32F407 MCU, which is based on a Cortex-M4 processor core running at 168 MHz, which includes a single-precision floating-point unit and 1 MB flash ROM. The robot dynamics are simulated on a PC, see the Appendix for details.

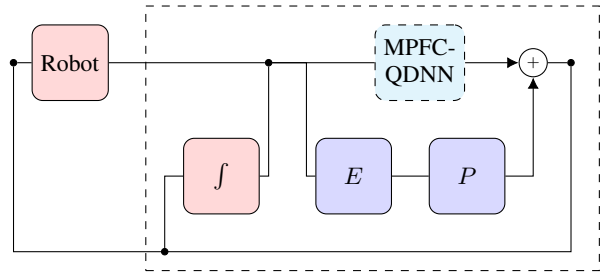
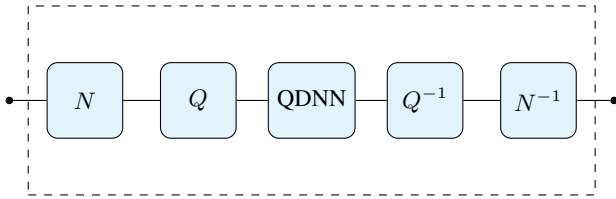
The QDNN consists of 9 hidden layers with roughly 4700 parameters, using 8-bit integers to store the parameters (i.e. 1 parameter requires 1 byte of ROM). The quantized parameter set  $\Theta$  requires less than 5 kB of the MCU's flash memory.

## V. RESULTS

As our reference implementation (denoted MPFC-OpEn), we use OpEn (the same solver used for training) to solve the MPFC problem (5). The advantages of MPFC are illustrated in Fig. 5. The input  $w$  computed by OpEn to steer the robot along the path in Fig. 6 shows that when the path curvature is tight, i.e. top ( $\theta = \frac{\pi}{2}$ ) and bottom ( $\theta = \frac{3\pi}{2}$ ) of the ellipse, the path speed  $v$  is reduced, and consequently the robot's forward speed  $s$  is also reduced. This allows the robot to follow the tight curve. Similarly,  $v$  is reduced when the constraints on  $s$  are active (e.g.  $\theta = \pi$ ) because the robot cannot otherwise closely follow the path.

The main advantage of using a DNN on an MCU is that it is relatively easy to implement quantization (8), inference (7), and dequantization (9) sequentially for all layers in the network. Furthermore, for a small network like the one used here (4700 parameters), the inference is executed much faster than solving the OCP (5).

Table I shows the execution time for different implementations of MPFC. Our experiments ran on a PC with Ubuntu



(a) The quantized deep neural network inference chain used to approximate the MPFC (denoted MPFC-QDNN on the right figure). (b) The proposed controller approach (MPFC-QDNN+P)

Fig. 4: Block diagram of the proposed combined controller. Inside the dashed block (MPFC-QDNN) is the MPFC controller approximated by a QDNN. The extended state  $z$  is fed into the MPFC-QDNN. The state is first normalized ( $\bar{z}$ ) then quantized ( $\hat{z}$ ), and finally fed into the QDNN block for inference of the approximate control input  $\hat{w}$ . Dequantization and denormalization are applied to get the approximated augmented control input  $w^D$ . The block  $E$  computes the robot's path error vector  $e$  (10) used by the P controllers. The vector  $w^P$  is added to  $w^D$  to compute the input  $w$ . The forward velocity  $s$ , and angular velocity  $\omega$  are applied to the robot, whereas the path velocity  $v$  is integrated to compute the path variable  $\theta$ .

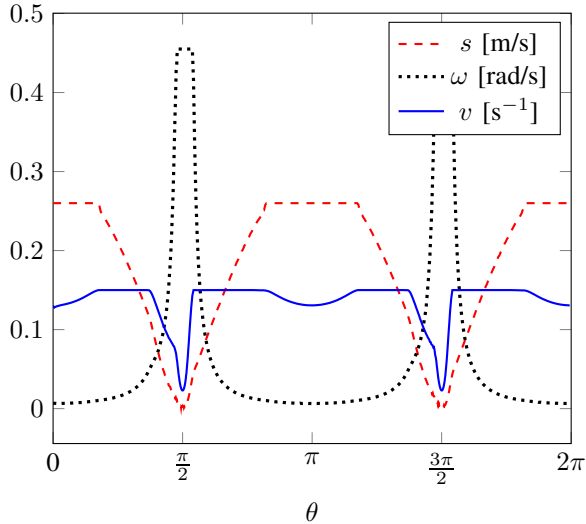


Fig. 5: Control inputs vs. path parameter. When the path curvature is tight (near  $\frac{\pi}{2}$ , and  $\frac{3\pi}{2}$ ) the path speed  $v$ , and the robot's forward speed  $s$  are reduced. The path speed  $v$  is also reduced when the input constraints are active (near  $\pi$ ).

Linux 22.04-LTS, and a x86-64 processor with a 2.4 GHz clock. Compared to MPFC-OpEn, the average execution time of the MPFC-QDNN+P implementation is about three orders of magnitude faster on the PC.

The QDNN implementation using 8-bit integers requires on average 230 microseconds to execute on the MCU. Currently, running OpEn on an MCU is not supported.

Fig. 6 shows a comparison of the path in the Cartesian  $XY$  plane followed by the simulated robot using different implementations. The absolute Cartesian position error is shown in Fig. 7, with a summary presented in Table II. All implementations can follow the path, with OpEn being the most accurate. When the worst-case error is considered, using a regular (non-quantized) DNN is two orders of magnitude worse than the OpEn implementation. The QDNN

Implementation	Mean [s]	Std. [s]	Worst [s]
OpEn (PC)	1.2E-3	5.9E-4	7.8E-3
QDNN+P (PC)	7.3E-6	2.9E-6	3.2E-5
OpEn (MCU)	-	-	-
QDNN+P (MCU)	2.3E-4	2.1E-6	2.4E-4

TABLE I: Mean, standard deviation (Std.), worst-case execution (Worst) time in seconds for 10000 steps close to the path. The table is split into MPFC implementations on a personal computer (PC, top part) and a microcontroller (MCU, bottom part). Note that the execution of QDNN+P on the MCU is temporally deterministic. In the PC case, the QDNN+P has more variability due to the operating system.

	Mean	Max.
OpEn	1.9E-4	3.3E-4
DNN	7.5E-3	2.1E-2
QDNN	1.6E-2	4.8E-2
QDNN+P	6.1E-4	4.9E-3

TABLE II: Mean and maximum Cartesian error in the path.

implementation has worse overall performance than the non-quantized network. Finally, the proposed addition of two P controllers to the QDNN reduces its worst-case error by an order of magnitude and outperforms the DNN.

## VI. CONCLUSIONS

The paper presented a model predictive path following implementation using quantized deep neural networks augmented with a controller for quantization error compensation. We showed a practical way to select the training set, and how to design the error compensation controller. Compared to a traditional MPFC using online optimization, our proposed approach requires only a fraction of the memory and runs several orders of magnitude faster on PC simulations. Although the path-following accuracy is slightly degraded, we believe the performance may still be good for low-cost applications. With a hardware-in-the-loop implementation



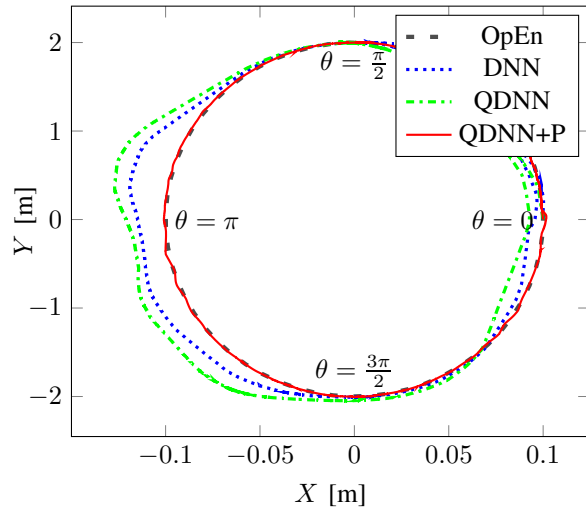


Fig. 6: The path followed by the robot using different MPFC implementations: OpEn (visually indistinguishable from the reference path  $p(\theta)$ ), the approximation using a deep neural network (DNN, 32-bit float), a quantized deep neural network (QDNN, 8-bit integer), and the proposed QDNN plus P control approach (QDNN+P).

using a microcontroller, we showed the effectiveness of this approach for low-cost embedded devices. Future work will discuss how to handle different path geometries with one trained QDNN and how to give performance guarantees.

#### APPENDIX

The hyperparameters of the QDNN network are the learning rate =  $4.5E-4$ , the activation function (ReLU), the number of hidden layers  $H = 9$ , and the units on each layer: input layer 4 units, followed by the hidden layers with 48, 16, 24, 16, 16, 40, 24, 16, and 24 units, and output layer 3 units.

The parameters of OCP (5) are the matrices  $Q = \text{diag}(2E5, 2E5, 1E5, 0)$ ,  $R = \text{diag}(1E1, 5E3, 1E5)$ , the box sets  $\mathcal{Z} = \{z \in \mathbb{R}^4 \mid \underline{z} \leq z \leq \bar{z}\}$ , with  $\underline{z} = [-5, -15, -\frac{\pi}{2}, -5]$ ,  $\bar{z} = [5, 15, \frac{\pi}{2}, -5]$ , and  $\mathcal{W} = \{w \in \mathbb{R}^3 \mid \underline{w} \leq w \leq \bar{w}\}$ , with  $\underline{w} = [-0.26, -0.455, 0]$ ,  $\bar{w} = [0.26, 0.455, 0.15]$ , the discretization time  $\delta = 0.01s$ , and the horizon length steps  $N = 60$ .

#### REFERENCES

- [1] H. Fukushima, T. Yanagiya, Y. Ota, M. Katsumoto, and F. Matsuno, "Model predictive path-following control of snake robots using an averaged model," *IEEE Transactions on Control Systems Technology*, vol. 29, no. 6, pp. 2444–2456, 2020.
- [2] T. Faulwasser, T. Weber, P. Zometa, and R. Findeisen, "Implementation of nonlinear model predictive path-following control for an industrial robot," *IEEE Transactions on Control Systems Technology*, vol. 25, no. 4, pp. 1505–1511, 2016.
- [3] M. W. Mehrez, K. Worthmann, G. K. Mann, R. G. Gosine, and T. Faulwasser, "Predictive path following of mobile robots without terminal stabilizing constraints," *IFAC-PapersOnLine*, vol. 50, no. 1, pp. 9852–9857, 2017.
- [4] T. Faulwasser and R. Findeisen, "Nonlinear model predictive control for constrained output path following," *IEEE Transactions on Automatic Control*, vol. 61, no. 4, pp. 1026–1039, 2015.

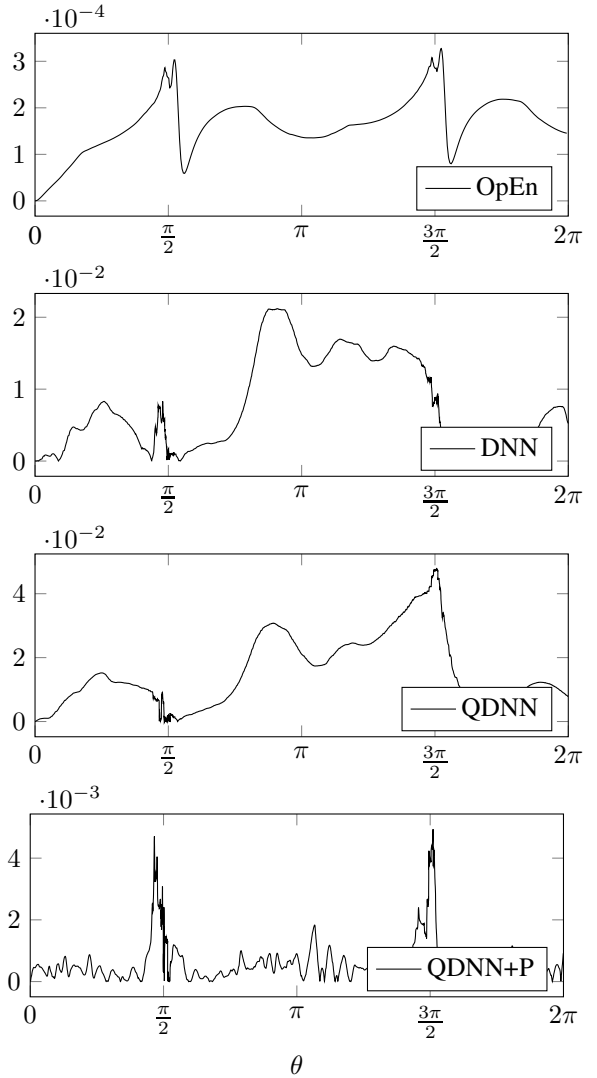


Fig. 7: Cartesian position error with respect to the reference path for different implementations. The MPFC solution as computed by OpEn is the most accurate. The next most accurate is the proposed approach (QDNN+P).

- [5] P. Sotasakis, E. Fresk, and P. Patrinos, "OpEn: Code generation for embedded nonconvex optimization," in *IFAC World Congress*, Berlin, Germany, 2020.
- [6] R. Verschuere, G. Frison, D. Kouzoupis, J. Frey, N. van Duijkeren, A. Zanelli, B. Novoselnic, T. Albin, R. Quirynen, and M. Diehl, "acados – a modular open-source framework for fast embedded optimal control," *Mathematical Programming Computation*, Oct 2021. [Online]. Available: <https://doi.org/10.1007/s12532-021-00208-8>
- [7] T. Parisini and R. Zoppoli, "A receding-horizon regulator for nonlinear systems and a neural approximation," *Automatica*, vol. 31, no. 10, pp. 1443–1451, 1995.
- [8] S. Lucia and B. Karg, "A deep learning-based approach to robust nonlinear model predictive control," *IFAC-PapersOnLine*, vol. 51, no. 20, pp. 511–516, 2018, 6th IFAC Conference on Nonlinear Model Predictive Control NMPC 2018. [Online]. Available: <https://www.sciencedirect.com/science/article/pii/S2405896318326958>
- [9] S. S. P. Kumar, A. Tulsyan, B. Gopaluni, and P. Loewen, "A deep learning architecture for predictive control," *IFAC-PapersOnLine*, vol. 51, no. 18, pp. 512–517, 2018.
- [10] A. Gholami, S. Kim, Z. Dong, Z. Yao, M. W. Mahoney, and K. Keutzer, "A survey of quantization methods for efficient neural network inference," *arXiv preprint arXiv:2103.13630*, 2021.

- [11] T. Faulwasser and R. Findeisen, "Nonlinear model predictive path-following control," in *Nonlinear model predictive control*. Springer, 2009, pp. 335–343.
- [12] P. Martin, R. Murray, and P. Rouchon, "Flat systems," in *Proc. of the 4th European Control Conf*, 1997, pp. 211–264.
- [13] T. Faulwasser, V. Hagenmeyer, and R. Findeisen, "Optimal exact path-following for constrained differentially flat systems," in *Proc. of 18th IFAC World Congress, Milano, Italy*, 2011, pp. 9875–9880.
- [14] M. Leshno, V. Y. Lin, A. Pinkus, and S. Schocken, "Multilayer feedforward networks with a nonpolynomial activation function can approximate any function," *Neural networks*, vol. 6, no. 6, pp. 861–867, 1993.
- [15] I. Goodfellow, Y. Bengio, and A. Courville, *Deep Learning*. MIT Press, 2016, <http://www.deeplearningbook.org>.
- [16] J. Bergstra and Y. Bengio, "Random search for hyper-parameter optimization." *Journal of machine learning research*, vol. 13, no. 2, 2012.
- [17] T. O'Malley, E. Bursztein, J. Long, F. Chollet, H. Jin, L. Invernizzi, *et al.*, "Kerastuner," <https://github.com/keras-team/keras-tuner>, 2019.
- [18] M. Abadi, P. Barham, J. Chen, Z. Chen, A. Davis, J. Dean, M. Devin, S. Ghemawat, G. Irving, M. Isard, *et al.*, "TensorFlow: a system for Large-Scale machine learning," in *12th USENIX symposium on operating systems design and implementation (OSDI 16)*, 2016, pp. 265–283.
- [19] F. Chollet *et al.*, "Keras," <https://keras.io>, 2015.